Metrology of laser-produced plasma light source for EUV lithography

N. R. Böwering*, J. R. Hoffman, O. V. Khodykin, C. L. Rettig, B. A. M. Hansson, A. I. Ershov, I. V. Fomenkov
Cymer Inc., 17075 Thornmint Court, San Diego, CA USA 92127-1712

ABSTRACT

Metrology concepts and related results are discussed for characterization of extreme ultraviolet (EUV) light sources based on laser-produced plasmas using metal foil and droplet targets. Specific designs of narrow-band EUV detectors employing multilayer mirrors and broadband detectors for droplet steering are described. Spatially resolved plasma imaging using in-band EUV pinhole cameras is discussed. A grazing-incidence flat-field EUV spectrometer is described that has been employed for spectroscopy in the 6 nm – 22 nm range. In addition, spectroscopic data of out-of-band radiation in the ultraviolet and visible spectral regions are presented. Results obtained for different wavelengths of the incident laser radiation and for both tin- and lithium foil- and droplet- targets are discussed.

Keywords: EUV metrology, EUV lithography, energy monitor, spectrometer, pinhole camera, spectral distribution, out-of-band radiation

1. INTRODUCTION

The manufacturers of exposure tools for extreme ultraviolet (EUV) lithography have agreed on a common set of specifications that have to be fulfilled by the light source used in such a tool[1]. Extensive metrology that has mainly to be performed at the EUV wavelength of choice of 13.5 nm is required in order to verify and optimize the source performance during development for both discharge- and laser-produced devices. Since the radiation source will be an integral part of the exposure tool its emission characteristics will directly influence the overall image quality. To evaluate and optimize the source performance completely a fairly large set of measurements has to be carried out, including collectable in-band power, angular distribution, stability and spectrum of the radiation, source size of the emitting plasma zone and lifetime. Thus, EUV metrology is an essential and critical task during light source development.

The corresponding metrology tools have been developed in parallel with the radiation sources during the past years at different places. A set of portable, so-called "flying circus" tools was first introduced by the group at the FOM institute[2,3] and some detection devices were designed and calibrated by other groups [4,5]. In recent years at Cymer, we have constructed, used and continuously improved a variety of devices to characterize our plasma focus discharge (DPF) source [6-9]. Improved and partially modified versions of these EUV metrology tools have now been applied to analyze the performance of our new laser-based plasma light sources. In this report we describe these tools and also present corresponding data obtained with them in investigations of our laser-produced plasma (LPP) devices.

2. EXPERIMENTAL ARRANGEMENT

In several different experiments the metrology tools were attached to ultra-high vacuum (UHV) chambers where a LPP was generated on thin tin and lithium foil targets and on tin droplets. To generate a micro-plasma a pulsed laser beam from a frequency-tripled Nd:YAG laser or a XeF excimer laser is focused by a lens through a window onto the target. The laser beam direction is parallel to the target normal and the spot size diameter on the order of 100 μm. A generic scheme of these arrangements is shown in figure 1. The target supports were mounted on 2-axis manipulators. A series of metrology tools is mounted to the chamber to analyze the radiation emitted from the plasma. The vacuum housings of the tools are separated by means of gate valves or shutters from the main chamber. In the case of foil targets the laser

* NBowering@cymer.com; phone 1 858 385-6287; fax 1 858 385-5353; cymer.com

Metrology, Inspection, and Process Control for Microlithography XIX,
edited by Richard M. Silver, Proc. of SPIE Vol. 5752 (SPIE, Bellingham, WA, 2005)
0277-786X/05/$15 · doi: 10.1117/12.600809

was normally operated in the single-pulse regime, for droplet targets the repetition rates were typically in the range of 10 Hz to 100 Hz. To characterize the angular distribution of the EUV radiation several detectors are mounted at different angles with respect to the incident laser beam direction.

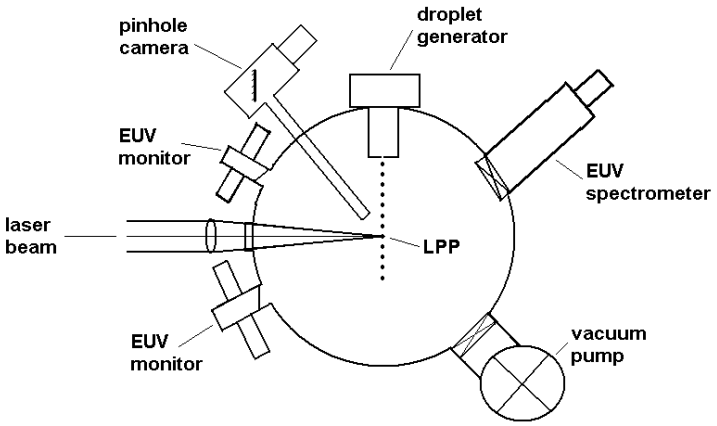

Figure 1: Scheme of laser-produced plasma with droplet target and diagnostic EUV metrology.

3. PHOTODIODE-BASED EUV PULSE ENERGY DETECTION

3.1 Narrow-band EUV monitors

For accurate measurement of the EUV pulse energy actinic metrology at the wavelength of choice, 13.5 nm, is required. For in-band EUV detection near 13.5 nm we use the combination of thin foil – multilayer mirror – silicon photodiode. The foils (typically 0.2 μm thick Zr or Nb or 1.0 μm thick Be) serve to suppress visible light and provide a broadband filtering of EUV radiation. They can be inserted into the beam path and easily exchanged. Since their transmission can be measured at repeated intervals we prefer the use of the fragile foils and do not use filter-coated photodiodes because there is no good possibility to measure the degradation in the latter case. For absolute radiation detection we use the well-characterized AXUV-100G photodiodes with known quantum efficiency at 91.8 eV photon energy, fairly high long-term stability and good linearity [4, 10, 11].

We have employed Mo/Si multilayer reflection mirrors for selection of the 13.5 nm band with either near-normal incidence or, in a more compact configuration, with a 45° angle of incidence. The normal-incidence configuration employs a series of apertures to reduce visible stray light produced mainly by scattered laser light (Fig.2). Two foils mounted on holders with separate UHV linear positioners can be inserted into the beam path. The filter foil transmission for the EUV band selected by the mirror is determined from a difference measurement with two and one foil while using another EUV detector for reference or employing sufficient pulse averaging. A CaF_2 window can be inserted to verify that pinholes are not present in the filter foils and that the remaining background light levels are very low. The EUV pulse energy is determined from the integrated photodiode signal (the accumulated charge) taking into account the 50 Ω sampling resistor, the quantum efficiency of the diode, the photon energy, the foil transmission, the mirror reflectivity and the geometrical factors (distance LPP – limiting aperture, size of limiting aperture). The effective bandwidth of the detection assembly obtained by convoluting the independently measured mirror reflectivity curve with the target material emission bandwidth is then rescaled to a 2% bandwidth value at 13.5 nm.

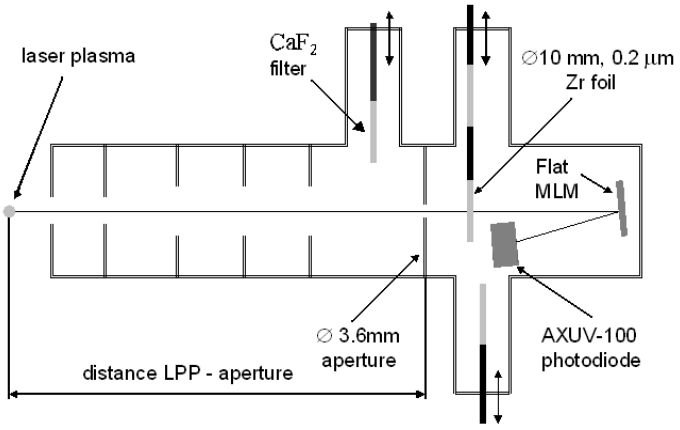

Figure 2: Schematics of EUV monitor with normal-incidence multilayer mirror and insertable filter foils

For use with droplet targets at higher LPP repetition rates we have devised the more compact scheme shown in figure 3. A fast pneumatic shutter protects the detector from debris when it is not in use. An aperture provides stray light suppression. Two foil holders on linear positioners each support two 10 mm diameter Zr filter foils and either a CaF_2 or glass filter. A limiting aperture of 5 mm diameter is mounted in front of a 45º Mo/Si multilayer mirror that directs the light onto a silicon photodiode (AXUV-100G) used with a reverse-bias of 50 volts. In connection with measurements of our discharge source we have previously described the use of a similar EUV detector with a 45º multilayer mirror and differentially pumped entrance aperture[9]. The actual level of in-band foil transmission is determined by difference measurements, similarly as described above. The CaF_2 or glass windows can be inserted for relative measurements of ultraviolet and visible radiation contributions or to verify the absence of pinholes in the filter foils and establish any remaining background levels. With the amplifier detection circuit used in this case the total charge during the signal pulse is accumulated and held by an integration capacitor for a period of a few microseconds during which it is digitized by an analog-to-digital converter. The digital signals are processed further on a pulse-by-pulse basis with a dedicated fast computer interface and by using Labview software.

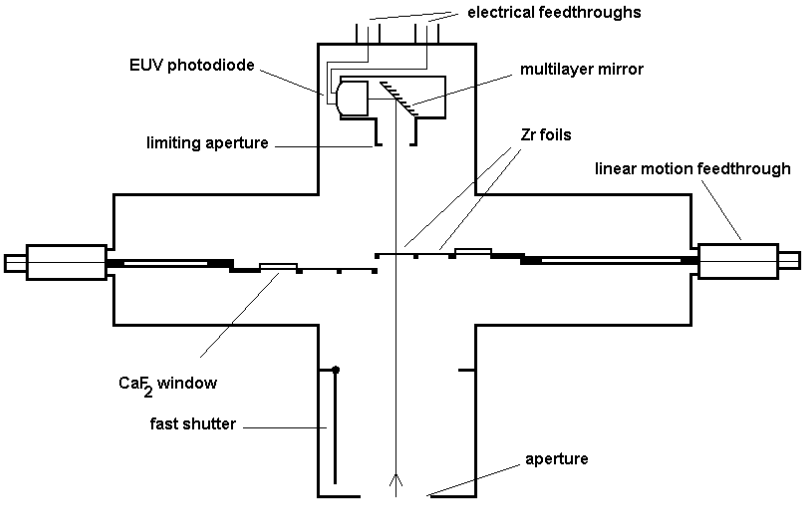

Figure 3: Schematics of EUV monitor with 45º multilayer mirror, insertable filters and fast shutter.

3.2 Broadband EUV monitors

For the purpose of centrally steering the laser beam onto the droplet target we have also employed a set of 4 broadband EUV detectors (without multilayer mirrors) arranged in steps of azimuthal angles of 90º with respect to the laser beam direction. They consist each of the combination debris shield – filter foil – photodiode. Out-of-center irradiation of a droplet by the laser beam results in an asymmetric distribution of EUV radiation and leads to different signal levels on the four photodiodes compared to the symmetric case. A debris shield is mounted in front of these detectors to mitigate the deposition of target material. Behind the shield, zirconium foils serve as broadband EUV filters and AXUV-100G photodiodes as radiation detectors. The integrated signals are converted to digital data as described above and processed by Labview software. The detector debris protection scheme was successfully tested at LPP repetition rates of up to 4 kHz. Steering of the deflection mirrors that direct the laser beam through the focusing lens onto the droplet target with closed-loop control is accomplished in an algorithm by comparing the relative signal levels at the four detectors with their corresponding detection sensitivity established from past data history.

4. EUV PINHOLE IMAGING

The actual size of the micro-plasma emitting the 13.5 nm radiation is of great importance for the amount of collectable light energy since the etendue directly influences the attainable collection efficiency [12]. In the recent years we have described several imaging techniques developed for measurements of the source size of our DPF sources [7-9]. We have used pinhole-camera arrangements with small pinholes, thin filter foils and EUV-sensitive CCD cameras [7] as well as direct-imaging configurations where the image was recorded with concave multilayer mirrors thus avoiding the influence of EUV diffraction at pinholes [8]. We then found that it is advantageous to combine the pinhole imaging with reflection at a multilayer mirror in order to achieve actinic metrology at 13.5 nm and eliminate the imaging of "hot spots" at x-ray wavelengths [9].

For characterization of LPP sources both pinhole- and direct-imaging techniques with high resolution are of interest. So far, we have employed the in-band pinhole-imaging technique. The experimental arrangements for source imaging consist of a 40 μm or 50 μm pinhole, a 0.2 μm Zr foil (placed right behind the pinhole), a 45º Mo/Si mirror and a backside-illuminated CCD camera (Roper-Scientific, array of 512 x 512 pixels of 24 μm size). Thin Si_3N_4 foils can be inserted into the beam path for attenuation, if necessary. Similarly to the case of the energy detectors, the Zr foils serve to block visible and other non-EUV radiation and the multilayer mirror selects only the in-band EUV light. In addition to the influence of the pixel size (which is small in magnifying imaging configurations), the object resolution is influenced by the combined effect of diffraction of EUV light at the pinhole and a geometric contribution depending on chosen pinhole size and magnification. To keep the resolution high it is advantageous if these two contributions are similar in magnitude. The lithium foil target was placed such that the pinhole arrangement viewed the target at a small grazing angle of no more than 5º in order to measure the plasma size in the z-direction normal to the target. Figure 4 shows a result of the EUV source image recorded for 460 mJ of incident laser energy focused to a spot size of ~80 μm diameter onto a 50 μm thick Li foil. The image was processed with proper angular rotation and analyzed by fitting an ellipse to the full-width-at-half-maximum (FWHM) contour of the image. In the case shown (355 nm laser wavelength, 8.5 ns FWHM pulse duration) this resulted in a source size of 140 μm by 110 μm.

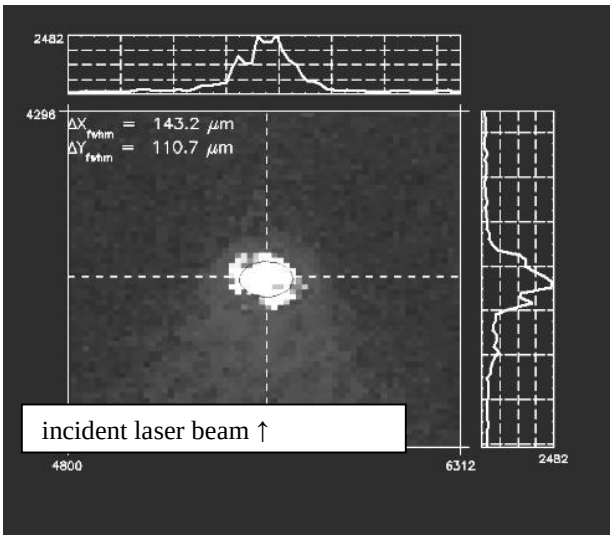

Figure 4: Pinhole camera image of the EUV source size from a 50 μm thick lithium foil target.

For imaging of the EUV plasma from tin droplets a pinhole arrangement with manual shutter in front of the pinhole was used. It was mounted at an angle of 90 º with respect to the incident XeF laser direction. The image was magnified by a factor of 3.2. Focusing the laser onto droplets of approximately 100 μm diameter produced symmetric images. Figure 5 shows a sequence of six consecutive laser plasmas generated at a repetition rates of 20 Hz and recorded during the read-out of the CCD camera. The incident laser energy was ~ 80 mJ in this case, the laser pulse duration was 25 ns FWHM, the laser wavelength is 351 nm. The diameter of the source size of the EUV emitting region is determined to be ~ 90 μm (FWHM) under these conditions. A series of such images can serve to determine the positional stability of the EUV emitting micro-plasma.

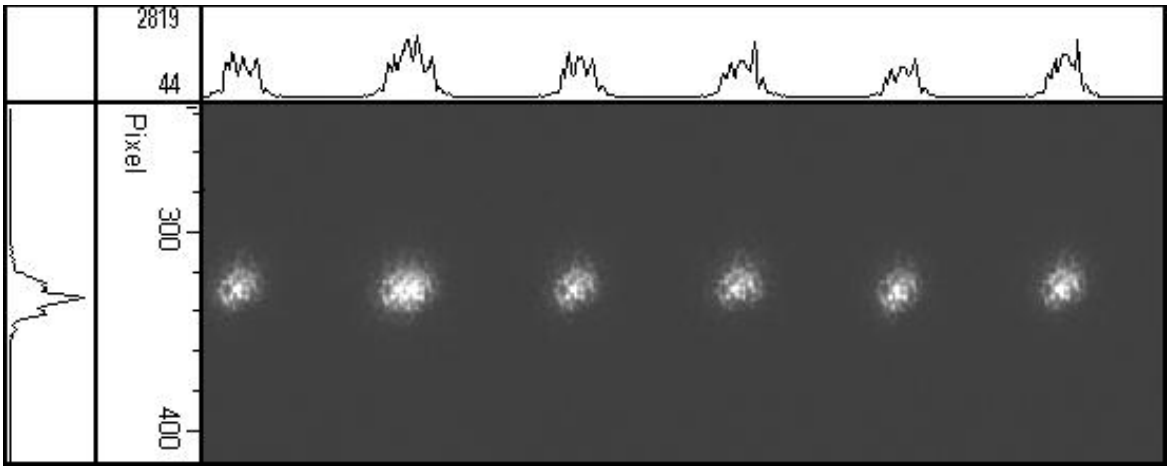

Figure 5: In-band EUV pinhole images of consecutive micro-plasmas from tin droplets generated with 351 nm laser light.

5. EUV SPECTROSCOPY

The EUV emission spectrum of the micro plasma is very sensitive to effective ion distribution and the plasma conditions reached. Analysis of the EUV spectra is particularly important in the case of LPP sources since changes of the laser intensity and also of the laser wavelength can lead to shifts in the spectra and to changes in the wavelength of

strongest EUV emission. For recording EUV spectra from our DPF sources we have previously used a high-resolution scanning-slit grazing-incidence spectrometer [6,13]. In order to obtain spectra with a single pulse we have also used transmission-grating spectrometer arrangements with CCD cameras [8,9,13]. However, usually only low spectral resolution can be obtained with the transmission gratings available. Using an aberration-corrected concave reflection grating with variable-line spacing (Hitachi grating # 001-0437) we have therefore constructed a flat-field imaging spectrometer [14,15] with an EUV sensitive CCD camera (Roper-Scientific, array of 1340 x 400 pixels of 20 μm size) as detector, similar to the design of Jenoptik[5]. A piezo-electric slit is used as entrance slit, a zirconium foil can be inserted for additional protection of the grating and the zero-order reflection is blocked in order to reduce the level of stray light to a minimum. The grating is mounted at a grazing incidence angle of 3º. With the rectangular CCD chip the spectral region from 6 nm – 22 nm can be covered. Wavelength calibration was carried out with xenon at a DPF source; a spectral resolution of up to $\lambda/\Delta\lambda = 500$ could be achieved.

Single-pulse and pulse-averaged spectra were recorded with tin and lithium LPP targets. For 50 μm thick foil targets of Sn and Li we have compared the resulting spectra for incident laser wavelengths of both 1064 nm and 355 nm at approximately 180 mJ pulse energy (see Fig. 6). For lithium line spectra are detected showing the first few members of the Lyman series of Li^{2+} as well as several lines of He-like lithium. Tin, on the other hand, gives rise to a quasi-continuous distribution of many lines from a range of different ionization states with 4d-4f transitions dominating[16]. The tin spectra are indicative of overlying absorption structures; opacity effects are clearly more pronounced for the 355 nm data. Some of the intense lines at longer wavelengths in the 1064 nm spectrum were identified as oxygen lines resulting from the oxidation of the foil. When going from 1064 nm to355 nm excitation, the critical plasma density increases and optical density effects are influential. This leads also to a slight shift of the effective maximum emission to near 13.0 nm for 355 nm laser wavelength.

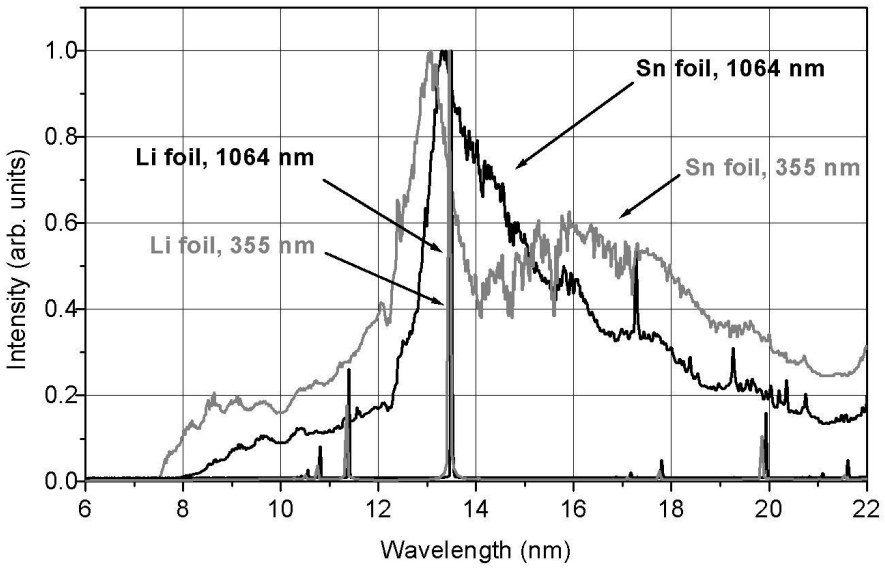

Figure 6: Single-pulse spectra from tin and lithium foil targets obtained at a laser wavelength of 1064 nm (black) and 355 nm (gray).

Figure 7 displays spectra from tin droplets with and without inserted 0.2 μm Zr foil using 351 nm XeF excimer laser radiation for LPP generation taken under slightly different laser focusing conditions. The laser pulse energy was ~ 100 mJ and the repetition rate was 20 Hz. Due to their relatively high EUV transmission in the region of 7 nm – 16 nm the zirconium foils can be employed for protection without serious loss of intensity. The tin droplet spectra are peaked at close to 13.5 nm, however, several absorption features are occurring in the 14 – 17 nm wavelength region.

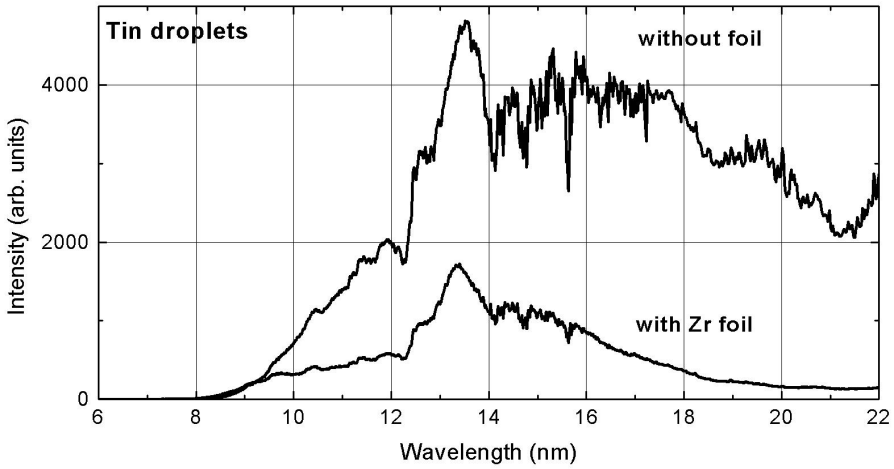

Figure 7: Spectra of laser-produced tin plasma using the flat-field spectrometer with and without protection foil.

6. OUT-OF-BAND MEASUREMENTS

We have several different metrology tools available to analyze the emitted radiation from the LPP outside the lithography band of 13.5 nm. The EUV spectrometer described above covers the EUV spectral region from 6 nm to ~ 22 nm. Emission in the ultraviolet and visible spectral range was studied by use of a corresponding spectrometer (Ocean Optics). Figure 8 shows corresponding spectra in the range of 200 nm – 800 nm obtained for tin and lithium targets using laser excitation at 355 nm. Clearly, the dominant contribution is scattered light of the incident laser radiation. In addition, there are numerous emissions, mostly from transitions of neutral atoms and singly ionized ions. In the case of tin, the number of transitions is much larger and the integral contribution is higher.

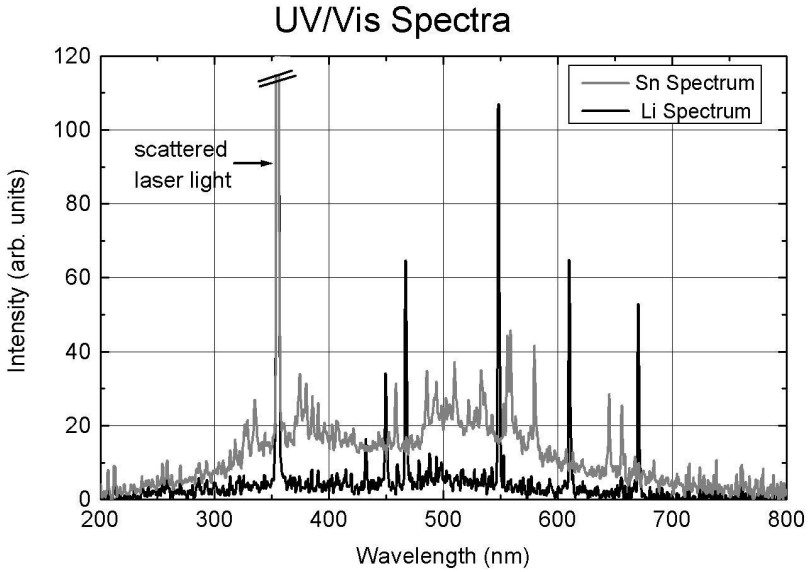

Figure 8: Ultraviolet – visible spectrum of emission from LPP lithium and tin targets. Note that the intensity of the scattered light of the 355 nm incident laser is off the scale.

A complimentary means to analyze out-of-band radiation is the use of different spectral filters in connection with EUV-sensitive photodiodes. To facilitate such measurements we have developed filter wheels where up to 8 filters, windows or pinholes can be rotated into the beam path in front of the photodiode. Filter combinations can also be employed when two wheels are used together. Typical filters are Zr, Nb, Si and Al foils as well as CaF_2, fused silica, BK7 and UV band-pass filters. They provide transmission windows for the emitted radiation in different spectral regions. A complication arises from the fact that the quantum efficiency of the photodiode varies also as a function of photon energy.

7. CONCLUSIONS

We have described different metrology tools for source characterization at EUV wavelengths and reported results obtained with our new LPP sources. Compared to tools previously used for analysis of our DPF discharge sources we have made significant progress. The tools can be used to assess a wide variety of source output parameters, including in-band output power, EUV pulse shape, pulse-to-pulse time-integrated EUV output energy, long-term energy stability, spectral emission distribution and spatial shape and stability of the plasma radiation. However, the detailed characterization of prototype EUV sources has only just started. As the source power levels are ever increasing and in-depth analysis needs to be carried out at the intermediate focus point, the requirements on the EUV metrology tools will become more demanding, and new developments will undoubtedly be necessary.

ACKNOWLEDGEMENTS

The authors gratefully acknowledge the invaluable support of other scientists, engineers and technicians involved in the EUV development at Cymer. We also acknowledge funding by DARPA during the initial phase of the work described here.

REFERENCES

1. K. Ota, Y. Watanabe, H. Franken, V. Banine, in: *Proc. Int. Sematech EUV Source Workshop, Santa Clara* (22 Feb. 2004).
2. R. Stuik, R. Constantinescu, P. Hegeman, J. Jonkers, H. Fledderus, V. Banine, and F. Bijkerk, in: *Proc. of SPIE Vol. **4146**, Soft X-Ray and EUV Imaging Systems*, W. M. Kaiser and R. H. Stulen, Eds., 121-127 (2000).
3. R. Stuik, F. Scholze, J. Tümmler, F. Bijkerk, Nucl. Instrum. Meth. **A 492**, 305-316 (2002).
4. F. Scholze, G. Brandt, P. Müller, B. Meyer, F. Scholz, J. Tümmler, K. Vogel, and G. Ulm, in: *Proc. of SPIE Vol. **4688***, 680-689 (2002).
5. M. C. Schürmann, T. Missalla, K. Mann, S. Kranzusch, R. M. Klein, F. Scholze, G. Ulm, R. Lebert, L. Juschkin, in: *Proc. of SPIE Vol. **5037**, Emerging Lithographic Technologies VII*, R. L. Engelstad, Ed., 378-388 (2003).
6. W. N. Partlo, I. V. Fomenkov, R. M. Ness, R. I. Oliver, S. T Melnychuk, and J. E. Rauch, in: *Proc. of SPIE Vol. **4343**, Emerging Lithographic Technologies V*, E. A. Dobisz, Ed., 232-248 (2001).
7. I. V. Fomenkov, R. M. Ness, I. R. Oliver, S. T. Melnychuk, O. V. Khodykin, N. R. Böwering, C. L. Rettig, J. R. Hoffman, in: *Proc. of SPIE Vol. **5037**, Emerging Lithographic Technologies VII*, R. L. Engelstad, Ed., 807-821 (2003).
8. I. V. Fomenkov, R. M. Ness, I. R. Oliver, S. T. Melnychuk, O. V. Khodykin, N. R. Böwering, C. L. Rettig, J. R. Hoffman, in: *Proc. of SPIE Vol. **5374**, Emerging Lithographic Technologies VIII*, R. S. Mackay, Ed., 168-182 (2004).
9. I. V. Fomenkov, N. Böwering, C. L. Rettig, S. T. Melnychuk, I. R. Oliver, J. R. Hoffman, O. V. Khodykin, R. M. Ness and W. N. Partlo, J. Phys. D: Appl. Phys. **37**, 3266-3276 (2004).
10. E. M. Gullikson, R. Korde, L. R. Canfield, and R. E. Vest, J. Electron Spectrosc. Rel. Phen. **80**, 313-316 (1996).
11. R. Stuik and F. Bijkerk, Nucl. Instrum. Meth. **A 489**, 370-378 (2002).

12. V. Banine and R. Moors, in: *Proc. of SPIE Vol. **4343**, Emerging Lithographic Technologies V*, E. A. Dobisz, Ed., 203-214 (2001).
13. N. Böwering, M. Martins, W. N. Partlo, and I. V. Fomenkov, J. Appl. Phys. **95**, 16-23 (2004).
14. T. Kita, T. Harada, N. Nakano, and H. Kuroda, Appl. Opt. **22**, 512-513 (1983).
15. N. Nakano, H. Kuroda, T. Kita, and T. Harada, Appl. Opt. **23**, 2386-2392 (1984).
16. G. O'Sullivan and R. Faulkner, Opt. Eng. **33**, 3978 (1994).